Performance of Tense Thin-Film Torsion Bar for Large Rotation and Low-Voltage Driving of Micromirror

doi: 10.1109/JSTQE.2007.892078

Performance of Tense Thin-Film Torsion Bar for Large Rotation and Low-Voltage Driving of Micromirror

Minoru Sasaki, Shinya Yuki, and Kazuhiro Hane

***Abstract*—In this paper, a micromirror device is developed by realizing the large rotation with the low-voltage driving. The maximum rotation angles observed at 5 V are 8.6° with hysteresis and 7° with little hysteresis at the static condition. The thin-film torsion bars contribute to decrease in the torsional spring constant. The tension is included for maintaining the compliance in the rotation of the mirror and for increasing stiffness in other movements. The performance of the torsion bar is investigated. The observed hard-spring effect is significant and this can be explained by the combination of the tension and the vertical displacement of the torsion bar.**

***Index Terms*—Electrostatic driving, low-voltage driving, micromirror, tension, thin-film torsion bar.**

I. Introduction

THE electrostatic driving is often used for micromirror devices. The electrostatic actuator is preferred, especially for the highly integrated mirror array [1]. The actuator consumes little power. The heat generation and the resultant degradation of the reliability can be prevented. The device can be completed within a chip, thereby making the integration easy. The limitation of the electrostatic driving is the difficulty in obtaining the large rotation angle with the low-voltage driving. Milanovic *et al*. [2] showed a design using the leverage for amplifying the mirror rotation from the lateral displacement of the actuator. Applying the driving voltage of 130 V, the static mirror rotation of 11° is achieved in the pulling mode. The eventual goal of the driving voltage would be to work under the power source of the existent system, for example, 5, 12, or 24 V. Limited devices satisfy this requirement. Hah *et al*. [3] reported the poly-Si micromirror fabricated by the surface micromachining. In one mirror design with the narrowest electrode gap, the rotation angle of 5.9° is obtained at 6 V for a single direction in plus and minus scan directions. As for the force for rotating mirror, the relatively large magnitude can be obtained using the vertical comb-drive actuator. As for the torsion bar for suspending the mirror, the structures are frequently designed with poly-Si film or thin crystal Si for decreasing torsional spring constant. The spring constant for the mirror rotation should be minimized while maintaining the rigidity in other motions. The serpentine spring helps the design, but often does not solve the problem completely [4]. In many cases, the pull-in instability occurs at the weakest direction, limiting the maximum rotation angle [3]. A group at Lucent Technologies reported a design with the so-called bearings for supporting the torsion bar against the vertical displacement [5]. As a new bearing material, a double-wall carbon nanotube is tested [6]. A group at Fujitsu Laboratories adopted the V-shaped torsion bar, which is stiff against the in-plane rotation [7]. Taking this advantage, the thick vertical combs can generate a larger driving force.

We have introduced the tense thin-film torsion bar for realizing low-voltage driving of the mirror, and confirmed its usefulness [8]. The tension is included in the torsion bar for increasing the rigidity against the unwanted mirror motion. In this study, the performance of the tense thin-film torsion bar is investigated.

Manuscript received September 29, 2006; revised November 8, 2006. This work was supported in part by the Japan Science and Technology Agency under Seeds Nourishment Test Research Grant 02-001 in 2004.

M. Sasaki is with the Department of Mechanical Systems Engineering, Toyata Technological Institute, Nagoya 468-8511, Japan (e-mail: mnr-sasaki@toyota-ti.ac.jp).

S. Yuki is with the Sony Corporation Micro Systems Network Company, Tokyo 141-0001, Japan (e-mail: shinya.yuki@jp.sony.com).

K. Hane is with the Department of Nanomechanics and the Department of Mechatronics and Precision Engineering, Tohoku University, Sendai 980-8579, Japan (e-mail: hane@hane.mech.tohoku.ac.jp).

Digital Object Identifier 10.1109/JSTQE.2007.892078

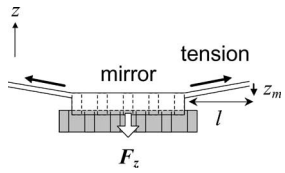

Fig. 1. Schematic of the micromirror for illustrating the effect of the tension inside the torsion bar for suppressing the vertical displacement.

II. Principle

Assuming that the torsion bar has a rectangular cross section, the torsional spring constant k_θ is expressed as follows:

$$k_\theta \approx \frac{Gwt^3}{3l}\left(1 - \frac{192}{\pi^5}\frac{t}{w}\tanh\frac{\pi w}{2t}\right) \tag{1}$$

where G is the shear modulus, l is the length of the torsion bar, w and t are the width or thickness, satisfying the condition $w > t$. When thin films are considered, t is the thickness. The factor t^3 shows that decrease in the value of t is effective for decrease in k_θ. The spring constant estimated from (1) is 1.4×10^{-11} Nm/rad, by setting values of G, l, w, and t as 80 GPa, 200 μm, 4 μm, and 0.3 μm, respectively. These values are typical of the thin-film torsion bar.

Fig. 1 shows the schematic for illustrating the effect of the tension inside the torsion bar. The tension works against the vertical displacement of the mirror. The tensile stress σ_0 inside

SiN film can be 760 MPa [9], and the tension $T = \sigma_0 wt$ is 910 μN for a cross section of 4 $\times 0.3$ μm ^{2}. This value is significantly large compared to the driving force of ~ 7 nN in our actuator design. Since the thin-film torsion bar is softest in the vertical direction, the vertical spring constant k_z becomes important. k_z is expressed as follows [10]:

$$kz \approx \frac{1}{\sum_{n=1,\,\mathrm{odd}}^{\infty} (1/l)[2/\{(Ewt^3/12)k_n^4 + \sigma_0 wtk_n^2\}]}$$
$$k_n = \frac{n\pi}{l}, \quad n = 1, 3, 5\,\Lambda \quad (2)$$

The elasticity E is set as 290 GPa for the calculation. When σ_0 is 0 and 760 MPa, k_z is 0.016 and 19 N/m, respectively. The large spring constant suppresses the vertical displacement of the mirror. The increase of the torsional spring constant $\Delta k_{\theta,\mathrm{stretch}}$ generated by the beam stretching can be estimated as follows (see Appendix for the deduction):

$$\Delta k_{\theta,\,\mathrm{stretch}} \approx \frac{wt}{l}\left\{\sigma_0\left(\frac{t^2}{24} + \frac{w^2}{24} + \frac{z_m^2}{6}\right) + \frac{Ez_m^2}{l^2}\left(\frac{t^2}{24} + \frac{w^2}{8} + \frac{z_m^2}{6}\right)\right\} + \theta^2 E\frac{wt}{l^3}\left\{\frac{t^4}{160} + \frac{t^2w^2}{144} + \frac{w^4}{160} + z_m^2\left(\frac{t^2}{12} + \frac{w^2}{36} + \frac{z_m^2}{10}\right)\right\} \quad (3)$$

where z_m is the vertical shift of the torsion bar that occurs with the mirror rotation. The magnitude of z_m is a few micrometers in our device, as described later. The term $(wt/l)\sigma_0\{(t^2/24) + (w^2/24) + (z_m^2/6)\}$ corresponds to stretching against the tension. The other terms correspond to the elastic stretching showing the linear dependence on the elasticity E. Comparing the magnitudes of $\sigma_0, E, w/l, t/l$, and z_m/l, the terms relating to the elastic stretching are found to be minor. There is another classification of terms in (3) based on the dependence on θ. One group does not depend on θ. Another group is proportional to θ^2 corresponding to the nonlinear factor against θ. Some values were evaluated by setting $z_m = 0$ for clearing the main feature of the thin-film torsion bar. The dominant part is the group relating to stretching against the stress σ_0 having the value of 3.1×10^{-12} Nm/rad. This is 22% of the spring constant estimated from (1). Without the vertical shift z_m, the tension is fundamentally perpendicular to the rotational displacement of the material inside the torsion bar. The increase of the spring constant is minimized. Notice that the dependence of $\Delta k_{\theta,\,\mathrm{stretch}}$ on t, expressed by (3), is different from that of k_θ expressed by (1). When the thickness t further decreases from 0.3 to 0.1 μm, $\Delta k_{\theta,\,\mathrm{stretch}}$ equals 1.0×10^{-12} Nm/rad, and Δk_θ becomes 0.53×10^{-13} Nm/rad. The relative magnitudes become reverse.

Fig. 2 shows the curves calculated based on (3). The thick and thin black curves show the sum of terms that are independent of θ and the contribution of $(wt/l)\sigma_0\{(t^2/24) + (w^2/24) + (z_m^2/6)\}$. The thick gray line at the bottom ($\sim 10^{-15}$ Nm/rad at maximum) is the sum of groups, which are proportional to θ^2. A mirror rotation of 5° is supposed at $z_m =$ 2.5 μm, keeping the linear relation. The magnitude is still subtle. Assuming $t \ll w$, the contribution of z_m in the terms $(wt/l)\sigma_0\{(t^2/24) + (w^2/24) + (z_m^2/6)\}$ will increase significantly when the condition $z_m > w/2$ is satisfied. Since the vertical displacement z_m is usually generated with the electrostatic force, the torsional spring constant k_θ will increase with the mirror rotation. The thin-film torsion bar has the nonlinear nature with the vertical displacement.

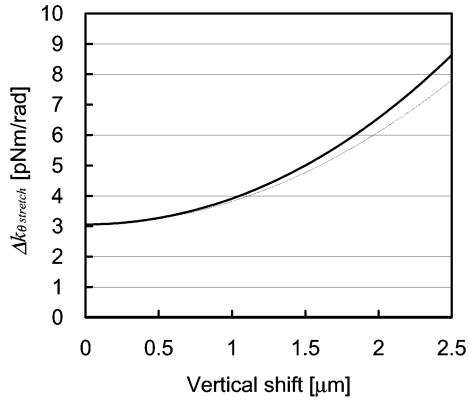

Fig. 2. Curves calculated based on (3). The thick and thin black curves are the sum of terms that are independent of θ and the contribution of $(wt/l)\sigma_0\{(t^2/24) + (w^2/24) + (z_m^2/6)\}$, respectively. The thick gray line at the bottom is the sum of terms proportional to θ^2.

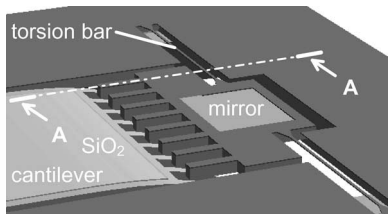

Fig. 3. Schematic for explaining the structure of the micromirror.

III. Fabrication

Fig. 3 shows a schematic of the device. The mirror has the moving comb. The fixed comb is at the end of the cantilever deflected downward. Fig. 4 shows the fabrication sequence illustrating the A–A cross section in Fig. 3. The device is fabricated from the silicon-on-insulator wafer. The thicknesses of device Si, buried oxide, and handle Si layers are 10, 2, and 200 μm, respectively. Si layers have the resistivity of 0.008–0.020 Ω cm. First, 1.7-μm-thick SiO_2 film is thermally grown. The oxide film will remain on the cantilever pattern. This oxide film later leads to the bending of the cantilever for realizing the vertical comb. The wafer is covered with SiN film grown by low-pressure chemical vapor deposition with a thickness of 460–500 nm (step 1), which is the condition required for obtaining the tensile film (850 °C, $SiH_2\ Cl_2/NH_3 = 5/10$ sccm, 350 Pa). After opening the contact holes in SiN film, the film thickness at the area around the torsion bar is adjusted to 300 nm (step 2). The backside of the handled Si layer is anisotropically plasma-etched for opening the space under the mirror (step 3). The backside pattern includes the fixing bar for connecting the

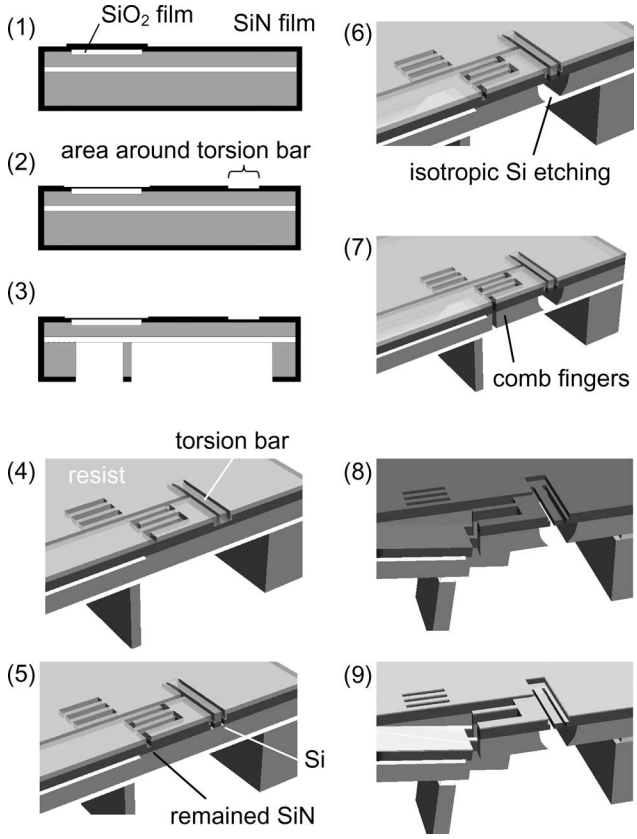

Fig. 4. Fabrication sequence of the micromirror with the thin-film torsion bar showing A–A cross section in Fig. 3.

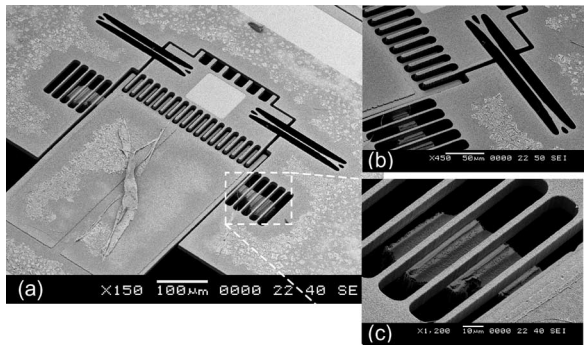

Fig. 5. (a) Fabricated micromirror. (b) Magnified image of the torsion bar and the vertical comb. (c) Grating besides the cantilever for controlling the release timing in the sacrificial SiO_2 etching.

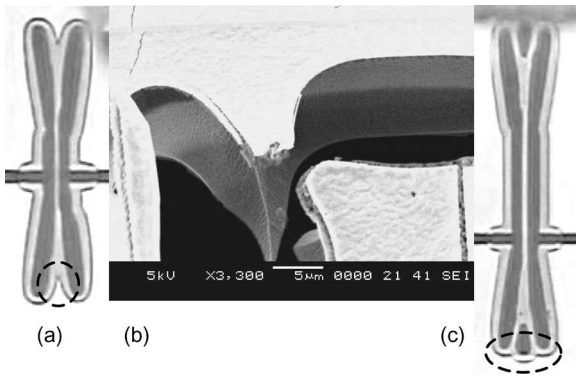

Fig. 6. (a) I-shaped torsion bar after the isotropic etching of the underlying Si. (b) Magnified image of the broken torsion bar. (c) Y-shaped torsion bar.

cantilever and the surrounding device layer. The role of this fixing bar is described later. The front side is patterned as the device shape including torsion bars, mirror, and combs with the photoresist (step 4). SiN film is plasma-etched. SiN film around the torsion bar is first removed and, hence, the underlying Si layer appears (step 5), since this region is thinner than the other area. At the area around the mirror and combs, SiN film remains. This film becomes the hard mask against the subsequent Si etching. The isotropic plasma etching of underlying Si is carried out for releasing the torsion bar (step 6). SiN film around mirror and combs also remains. The selectivity of Si/SiN is $\sim$140. After the plasma-etching of SiN film around the comb fingers, structures of mirror and combs are prepared by the anisotropic plasma-etching (step 7). The photoresist patterned at step 4 remains. When the sacrificial SiO_2 layer is removed, the mirror is released. As shown in Fig. 3, the fixed comb is at the end of the cantilever, which bends by the compress stress inside SiO_2 film [11]. The vertical comb drive actuator is, then, realized. After ashing out the photoresist (step 8), Au/Cr film is deposited (step 9). This metal film gives the electrical connection to the mirror across SiN insulating torsion bar. The connection to the Si layer of the device is obtained through the contact hole prepared in step 2.

Fig. 5(a) shows the fabricated bulk mirror suspended by the thin-film torsion bars. The size of the torsion bar is 200 μm $\times$ 4 μm $\times$ 0.3 μm. The surface roughness is attributed to the attack of HF vapor on SiN film during the sacrificial layer etching. Fig. 5(b) shows the magnified image of the torsion bar and the vertical comb. By controlling the length of the cantilever, three different comb-to-comb differences (8.2, 13, and 20 μm) are prepared. The mirror is designed for protecting the torsion bar against the load that can be applied during the process. The fixed comb is at the end of the cantilever, which deflects after the sacrificial SiO_2 layer etching. This deflection should occur after the release of the mirror. If the connection remains between the cantilever and the mirror, the load due to the cantilever deflection is applied to the torsion bar. The release timing has to be controlled. Beside the cantilever, gratings are prepared as shown in Fig. 5(c). Beneath this grating, there is the fixing bar prepared at the fabrication step 3. When the sacrificial SiO_2 layer is removed, this fixing bar is released, allowing the deflection of the cantilever. During the vapor HF-etching process, this front-side grating will be under a condition similar to that of the comb fingers. The width of the grating bar is 4 μm, and the comb gap is of the same size. The sacrificial layer around the comb structure is etched from both front and back sides with HF vapor. The fixing bar needs longer time for the release compared to the comb structures.

Two torsion bars are designed. The first one has a simple I-shape, as shown in Fig. 6(a). When the isotropic underetching proceeds in the fabrication step 6, underlying Si profile has the sharp apex at the root of the torsion bar, as shown by the dashed circle. The torsion bar breaks frequently at around this

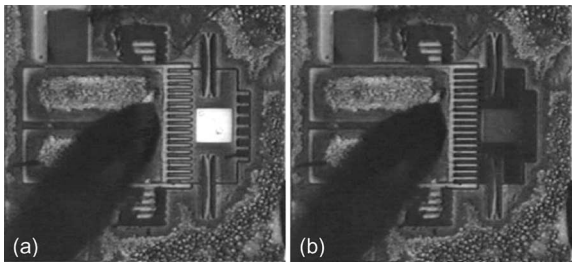

Fig. 7. Optical micrographs of micromirror. (a) Driving voltage = 0 V. (b) Driving voltage = 3 V.

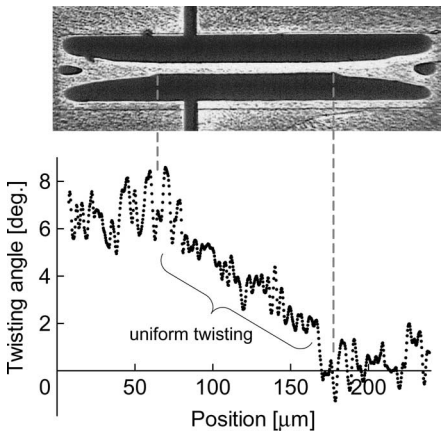

Fig. 8. Twisting angle of the torsion bar measured along the length. The inserted micrograph shows the corresponding position of the torsion bar.

apex, as shown in Fig. 6(b). This can be attributed to the stress concentration. The second design has a Y-shape, as shown in Fig. 6(c). The underlying Si profile becomes rounded. The yield of the device improves. The following results are obtained from the device with this design. For protecting the mirror from the electromagnetic noise, the actuator electrodes are electrically shorted with the bridge similar to the torsion bar. This bridge is cut just before the experiments.

IV. Results

Fig. 7(a) and (b) shows optical micrographs when the driving voltages are 0 and 3 V, respectively. The mirror is grounded. The brightness of the mirror changes showing the mirror rotation. Due to the high sensitivity to the electrical field of the mirror, the electromagnetic noise has a significant effect. Grounding the surrounding elements is necessary for stabilizing the mirror rotation. The brightness of the torsion bar changes from bright to dark color indicating the twisting of the torsion bar. Fig. 8 shows the twisting angle measured along the torsion bar. The inserted micrograph shows the corresponding position of the torsion bar. The driving voltage of 7 V is applied keeping the steady balance and the profile of the torsion bar is measured using the optical confocal microscope. Since the beam spot is ~ 4 μm in diameter under 50$\times$ objective, 4-μm-wide torsion bar is difficult to measure the profile. Fig. 8 is obtained from 8-μm-wide torsion bar. The distribution of the twisting angle along the torsion bar is calculated from the height difference across the width cross section. The surface roughness on the device surface is also one of the reasons for noise. The data show the uniform twisting of the torsion bar. Y-shaped branches show little twisting.

The relation between the mirror rotation angle and the tension inside the torsion bar is investigated. The tension is decreased by the compress stress added by the implantation of boron ion in the film. When the dose is 3.2×10^{14} atoms/cm^2 at an acceleration of 70 keV, the tensile stress decreases to 83% of the origial value. With the additional dose of 1.0×10^{15} atoms/cm ^{2} at 130 keV to the same wafer, the stress decreases to 52% of the origial value. These values of the tensile stress are monitored using the strain gauge [12]. Supposing the elasticity of SiN film to be 290 GPa [13], the estimated stress and the original tension are 780 MPa and 940 μN, respectively.

Fig. 9 shows a series of the mirror rotation angle as the function of the driving voltage showing the round trip motions. The angle measurement is carried out using the optical lever method as shown by the inset. The laser beam spot reflected from the mirror is measured using the position sensitive detector. The sweeping frequency of the driving voltage is 2 Hz. The initial comb-to-comb height distances of the vertical comb are different in Fig. 9(a)–(c). Fig. 9(a) is obtained when the initial comb-to-comb distance is 8.2 μm. Combs overlap each other vertically from the beginning as shown in the inset. The mirror rotation is generated from the lower voltage. The curve of 100% tension is rather linear. With the decrease of the tension, the rotation angle saturates at the higher voltage. The saturated angle is largest for torsion bar with 52% tension. This can be explained by the decrease of the torsional spring constant. Notice that the curve of 83% tension shows the larger rotation angle at the driving voltage of ~ 0.5 V. The curve shape is rather trapezoid. When the tension decreases to 52%, the curve becomes S-shaped. Fig. 9(b) shows the case when the comb-to-comb distance is 13 μm, with the vertical gap of 3 μm as shown in the inset. Compared to the case of Fig. 9(a), a larger rotation angle is obtained. With the decrease of the tension, S-shaped curves start to show hysteresis. The value of 83% tension shows the largest rotation angle of 8.6 $^\circ$ at 5 V. For 52% tension, the rotation angle decreases to 7.5 $^\circ$ at 5 V. This can be explained by the larger vertical displacement of the mirror instead of the rotation. In the region < 1 V, three curves show similar rotation angle. Fig. 9(c) shows the case when the comb-to-comb distance is 20 μm, with the vertical gap of 10 μm as shown in the inset. The electrode condition becomes similar to that of the parallel plate. The saturated rotation angle of 83% tension is again larger than that of 52% tension. The curves with decreased tension show the pull-in phenomenon. The pull-in voltage of 83% tension (3.0 V) is larger than that of 52% tension (2.4 V). The stably obtainable rotaion angle before the pull-in is 7 $^\circ$ and 3.5 $^\circ$ for 83% and 52% tensions, respectively. For 52% tension, the rotaion angle of 3.5 $^\circ$ is nearly one-third of the saturated angle of 10.4 $^\circ$. The tension of 100% keeps the mirror stable up to 5 V and 7 $^\circ$. The tension inside the torsion bar increases the stable region. The curve of 100% tension is still rather linear. This is advantageous for controlling the rotation angle. The hysteresis in the

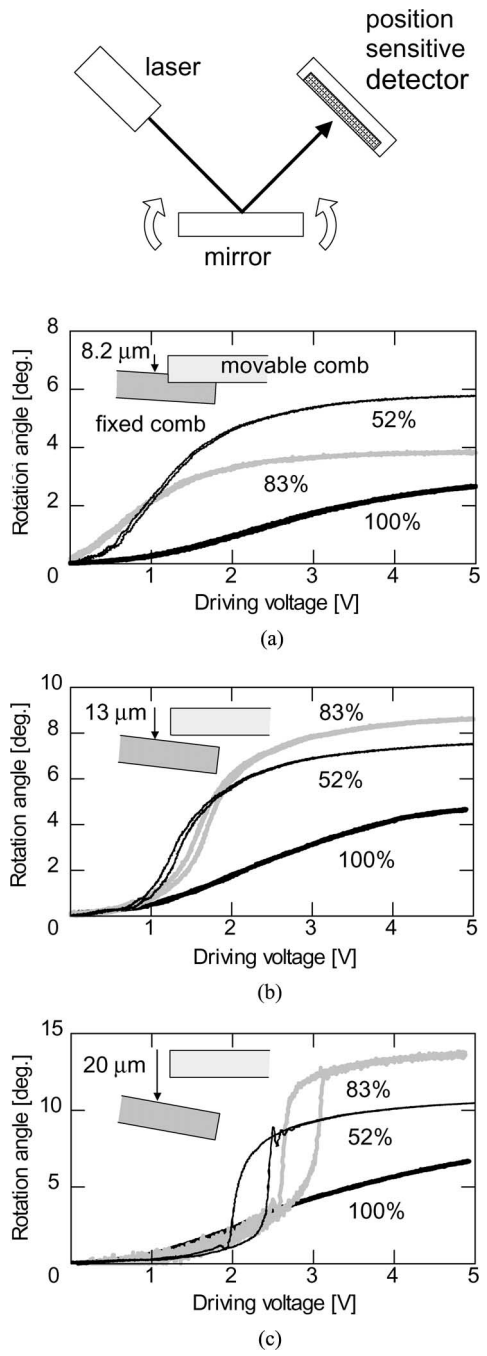

Fig. 9. Mirror rotation angle as a function of the driving voltage, with different initial comb-to-comb distances. (a) 8.2 μm. (b) 13 μm. (c) 20 μm. Thick black, thick gray, and thin black curves correspond to 100%, 83%, and 52% tensions, respectively.

round trip motion seems to be small with 100% tension. At the voltage of $\sim$ 2 V, the torsion bar with 100% tension shows the largest rotation angle.

Fig. 10 shows the vertical displacement of the mirror. The confocal microscope is used. The measured device has the comb-to-comb height difference of 8.2 μm. When the tension is original 100%, the vertical shif is < 0.8 μm at 7 V. The vertical displacement increases rather linearly indicating that this is inevitable magnitude. With the decrease of the tension, the magnitude of

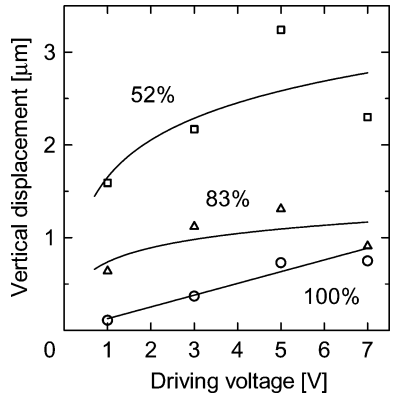

Fig. 10. Vertical displacement of the mirror supported by the torsion bars with 100%, 83%, and 52% tensions.

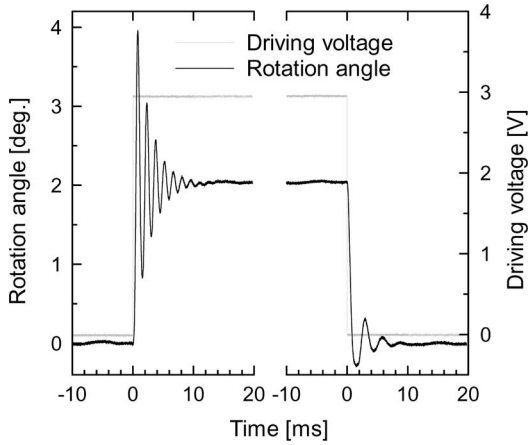

Fig. 11. Step response of the micromirror. The driving voltage is 3 V. The device has 8.2-μm comb-to-comb height difference between combs and 100% tension in the torsion bar.

the vertical displacement increases. When the tension is 83 or 52%, the vertical displacement soon increases even at 1 V and saturates at the larger driving voltage. Since the torsion bar is thin, the vertical displacement is generated even at the lower driving voltage. This means that the effect of the tension is significant at the lower driving voltage.

Fig. 11 shows the step response. The step height of the driving voltage is 3 V. The comb-to-comb distance is 8.2 μm. The tension is original 100%. The overshoot oscillation is observed. The ringing periods are 1.5 ms (corresponding to 670 Hz) and 2.8 ms (corresponding to 360 Hz) for the rise up and the fall down steps, respectively. The increased ringing frequency at the rise up step can be explained by the hard-spring effect of the torsional spring constant. This increasing ratio is significantly large compared to the case using usual crystal Si torsion bar. Filhol *et al.* [14] reported $\sim$ 0.63% increase of the resonant frequency when the mirror rotates by 50° using the torsion bar having dimensions of 8.5-μm width, 20-μm thickness, and 400-μm length without tension inside [14]. This is the hard-spring effect caused by E. These features agree with the evaluation using (3). The nonlinear terms proportional to θ^2 have small values compared to other terms. Although the increasing ratio

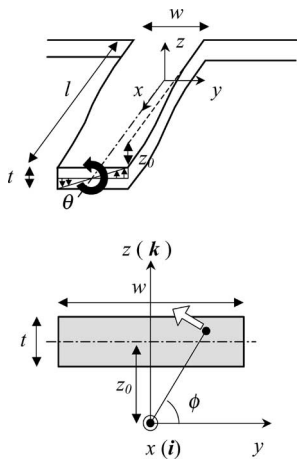

Fig. 12. Calculation model of the thin-film torsion bar.

of the torsional spring constant evaluated from (3) is relatively small compared to the observed value, the change of the magnitude is reasonable. The curves of the rotation angle with 100% tension in Fig. 9(a)–(c) are rather linear showing similar shapes. The hard-spring effect is considered to cancel the nonlinearity of the electrostatic actuator to some extent.

V. Conclusion

An electrostatically driven micromirror device is developed realizing the low-voltage driving. The thin-film torsion bar can decrease the torsional spring constant significantly. With the tension, the thin-film torsion bar can be stiff against the vertical displacement maintaining the compliance with the mirror rotation. The increase of the torsional spring constant is considered taking the tensile stress σ_0 and the vertical shift z_m account. The vertical shift is generated with the mirror rotation, and the thin-film torsion bar shows the large hard-spring effect, which is the unique characteristic. The stably obtainable rotation angle is increased with the tension. The observed rotation angles at 5 V are 8.6 ° with hysteresis, and 7 ° with little hysteresis at the static condition.

Appendix

The deduction of (3) is based on the energy method. Fig. 12 shows the calculation model of the thin-film torsion bar. For considering the stretching along x-axis (length direction), the change in length ds of the torsion bar can be expressed (4), shown at the bottom of the page. The displacements along x-, y-, and z-axis are expressed by u, v, and w, respectively; u is the axial displacement, and v and w are transversive displacements. Considering the displacement of the torsion bar, the axial strain ε_x can be obtained as follows [10]:

$$\varepsilon_x = \frac{ds - dx}{dx} \approx \frac{du}{dx} + \frac{1}{2}\left(\frac{dv}{dx}\right)^2 + \frac{1}{2}\left(\frac{dw}{dx}\right)^2. \quad (5)$$

The coordinate is shown in Fig. 12. The displacement $\boldsymbol{r}$ at point (x, y, z) inside the torsion bar generated by the mirror rotation θ can be expressed as follows:

$$\boldsymbol{r} \approx z_0\boldsymbol{k} + \frac{\theta x}{l}\sqrt{y^2 + (z+z_0)^2}(-\sin\phi\boldsymbol{j} + \cos\phi\boldsymbol{k}) \quad (6)$$

where θ is the mirror rotation angle at the end of the torsion bar. As seen from the dependence on θ and x, this equation assumes the uniform twisting of the torsion bar, which is justified by the data of Fig. 8. The axial displacement u is set to zero. $\boldsymbol{j}$ and $\boldsymbol{k}$ are unit vectors for y- and z-axis, respectively. This includes the offset z_0 between the center of the mirror rotation and the center of the cross section of the torsion bar. The rotation radius is $\sqrt{y^2 + (z+z_0)^2}$. Considering the relations $\sin\phi = (z+z_0)/\sqrt{y^2+(z+z_0)^2}$, $\cos\phi = y/\sqrt{y^2+(z+z_0)^2}$, (6) can be rewritten as follows:

$$\boldsymbol{r} \approx z_0\boldsymbol{k} + \frac{\theta x}{\boldsymbol{l}}\{-(z+z_0)\boldsymbol{j} + y\boldsymbol{k}\}. \quad (7)$$

Comparing to the directions, we can assign u, v, and w as follows:

$$\begin{aligned} u(x) &= 0 \\ v(x) &= -\frac{\theta x}{l}(z+z_0) \\ w(x) &= z_0 + \frac{\theta x y}{l}. \end{aligned} \quad (8)$$

The vertical deflection z_0 is set as follows, thereby making the calculation simple:

$$z_0 \approx \frac{z_m}{l}(l-x). \quad (9)$$

Although this supposition is not strict, the characteristic will be included. Here, z_0 is 0 at the mirror end $(x = l)$, and z_0 is z_m at the base $(x = 0)$. Substituting this function in (8), the strain ε_x can be obtained using (5) as follows:

$$\varepsilon_x = \frac{\theta^2}{l^2}\left\{\frac{z^2}{2} + \frac{z_m z}{l}(l-2x) + \frac{z_m^2}{2l^2}(l-2x)^2 + \frac{y^2}{2}\right\} - \frac{\theta z_m y}{l^2} + \frac{z_m^2}{2l^2}. \quad (10)$$

$$\begin{aligned} ds &= \sqrt{[dx + u(x+dx) - u(x)]^2 + [v(x+dx) - v(x)]^2 + [w(x+dx) - w(x)]^2} \\ &= \sqrt{\left[1 + \frac{du}{dx}\right]^2 + \left[\frac{dv}{dx}\right]^2 + \left[\frac{dw}{dx}\right]^2} \\ &\approx dx\left[1 + \frac{du}{dx} + \frac{1}{2}\left(\frac{dv}{dx}\right)^2 + \frac{1}{2}\left(\frac{dw}{dx}\right)^2\right]. \end{aligned} \quad (4)$$

The strain energy can be found as follows:

$$W_{\text{stretch}} = \frac{1}{2}\int \sigma_x \varepsilon_x dV = \frac{1}{2}\int (\sigma_0 + E\varepsilon_x)\varepsilon_x dV$$
$$= \frac{\theta^2}{2}\frac{wt}{l}\left\{\sigma_0\left(\frac{t^2}{24}+\frac{w^2}{24}+\frac{z_m^2}{6}\right)+\frac{Ez_m^2}{l^2}\left(\frac{t^2}{24}+\frac{w^2}{8}+\frac{z_m^2}{6}\right)\right\}$$
$$+\frac{\theta^4}{4}E\frac{wt}{l^3}\left\{\frac{t^4}{160}+\frac{t^2w^2}{144}+\frac{w^4}{160}+z_m^2\left(\frac{t^2}{12}+\frac{w^2}{36}+\frac{z_m^2}{10}\right)\right\} \tag{11}$$

The work done by the external load is $T_{\text{stretch}}\theta$. T_{stretch} is the additional torque occurred by the stretching. We find the total potential energy to be as follows:

$$U = W_{\text{stretch}} - T_{\text{stretch}}\theta. \tag{12}$$

Taking the derivative with respective to θ, setting to zero yields T_{stretch}:

$$T_{\text{stretch}} = \frac{\partial W_{\text{stretch}}}{\partial\theta} = \theta\frac{wt}{l}\left\{\sigma_0\left(\frac{t^2}{24}+\frac{w^2}{24}+\frac{z_m^2}{6}\right)\right.$$
$$\left.+\frac{Ez_m^2}{l^2}\left(\frac{t^2}{24}+\frac{w^2}{8}+\frac{z_m^2}{6}\right)\right\}$$
$$+\theta^3 E\frac{wt}{l^3}\left\{\frac{t^4}{160}+\frac{t^2w^2}{144}+\frac{w^4}{160}\right.$$
$$\left.+z_m^2\left(\frac{t^2}{12}+\frac{w^2}{36}+\frac{z_m^2}{10}\right)\right\}. \tag{13}$$

From this relation, we can obtain (3) by defining $\Delta k_{\theta,\,\text{stretch}} = T_{\text{stretch}}\theta$.

ACKNOWLEDGMENT

The Micro/Nano-Machining Research and Education Center, Tohoku University, is gratefully acknowledged for providing the facilities for this research.

REFERENCES

[1] P. F. Van Kessel, L. J. Hornbeck, R. E. Meier, and M. R. Douglass, "A MEMS-based projection display," *Proc. IEEE*, vol. 86, no. 8, pp. 1687–1704, Aug. 1998.

[2] V. Milanovic, M. Last, and K. S. J. Pister, "Laterally actuated torsional micromirrors for large static deflection," *IEEE Photon. Technol. Lett.*, vol. 15, no. 2, pp. 245–247, Feb. 2003.

[3] D. Hah, S. T. Huang, J. Tsai, H. Toshiyoshi, and M. C. Wu, "Low-voltage, large-scan angle MEMS analog micromirror arrays with hidden vertical comb-drive actuators," *J. Microelectromech. Syst.*, vol. 13, pp. 279–289, Apr. 2004.

[4] G. Barillaro, A. Molfese, A. Nannini, and F. Pieri, "Analysis, simulation and relative performance of two kinds of serpentine springs," *J. Micromech. Microeng.*, vol. 15, pp. 736–746, Feb. 2005.

[5] V. A. Aksyuk, F. Pardo, D. Carr, D. Greywall, H. B. Chan, M. E. Simon, A. Gasparyan, H. Shea, V. Lifton, C. Bolle, S. Arney, R. Frahm, M. Paczkowski, M. Haueis, R. Ryf, D. T. Neilson, J. Kim, C. R. Giles, and D. Bishop, "Beam-steering micromirrors for large optical cross-connects," *J. Lightw. Technol.*, vol. 21, no. 3, pp. 634–642, Mar. 2003.

[6] A. M. Fennimore, T. D. Yuzvinsky, W.-Q. Han, M. S. Fuhrer, J. Cuming, and A. Zettl, "Rotational actuators based on carbon nanotubes," *Nature*, vol. 424, pp. 408–410, Jul. 2003.

[7] M. Yano, F. Yamagishi, and T. Tsuda, "Optical MEMS for photonic switching—Compact and stable optical crossconnect switches for simple, fast, and flexible wavelength applications in recent photonic networks," *IEEE J. Sel. Topics Quantum Electron.*, vol. 11, no. 2, pp. 383–394, Mar./Apr. 2005.

[8] M. Sasaki, S. Yuki, and K. Hane, "Large-rotation and low-voltage driving of micromirror realized by tense thin film torsion bar," *IEEE Photon. Technol. Lett.*, vol. 18, no. 15, pp. 1573–1575, Aug. 2006.

[9] M. Sekimoto, H. Yoshihara, T. Ohkubo, and Y. Saitoh, "Silicon nitride single-layer X-ray mask," *Jpn. J. Appl. Phys.*, vol. 20, pp. L669–L672, Sep. 1981.

[10] S. D. Senturia, *Microsystem Design*. New York: Springer/Business Media, ch. 9.

[11] M. Sasaki, D. Briand, W. Noell, N. de Rooij, and K. Hane, "Three-dimensional SOI-MEMS constructed by buckled bridges and vertical comb drive actuator," *IEEE J. Sel. Topics Quantum Electron.*, vol. 10, no. 3, pp. 455–461, May/Jun. 2004.

[12] L. Lin, A. P. Pisano, and R. T. Howe, "A micro strain gauge with mechanical amplifier," *J. Microelectromech. Syst.*, vol. 6, pp. 313–321, Dec. 1997.

[13] O. Tabata, K. Kawahata, S. Sugiyama, and I. Igarashi, "Mechanical property measurements of thin films using load-deflection of composite rectangular membranes," *Sens. Actuators*, vol. 20, pp. 135–141, Nov. 1989.

[14] F. Filhol, E. Defay, C. Divoux, C. Zinck, and M.-T. Delaye, "Resonant micro-mirror excited by a thin-film piezoelectric actuator for fast optical beam scanning," *Sens. Actuators*, vol. A123-24, pp. 483–489, Sep. 2005.

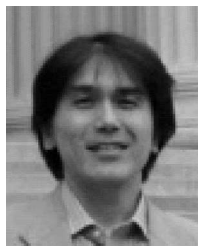

Minoru Sasaki received the M.S. degree in electromechanics and Dr. Eng. degree in electronics from Nagoya University, Nagoya, Japan, in 1993 and 1995, respectively.

During 1996, he was a Research Fellow with the Japan Society for the Promotion of Science. Since 1996, he was a member of the Department of Mechatronics and Precision Engineering, Tohoku University, Sendai, Japan. Since 2007, he has been a professor in the Department of Mechanical Systems Engineering, Toyota Technological Institute, Nagoya, Japan. His current research interests include optical MEMS including sensors.

Shinya Yuki received the M.S. degree in nanomechanics engineering from Tohoku University, Sendai, in 2005.

Since 2005, he has been with the Sony Corporation Micro Systems Network Company, Tokyo, Japan.

Kazuhiro Hane received the M.S. and Dr. Eng. degrees in electronics from Nagoya University, Nagoya, Japan, in 1980 and 1983, respectively.

From 1983 to 1994, he was with the Department of Electronic–Mechanical Engineering, Nagoya University. From 1985 to 1986, he was a Guest Researcher at the National Research Council of Canada. Since 1994, he has been a Professor with the Department of Mechatronics and Precision Engineering, Tohoku University, Sendai, Japan. His current research interests include microsensors and optomechanical systems.